TAPERED DOUBLE CANTILEVER BEAM FRACTURE TESTS OF PHENOLIC-WOOD ADHESIVE JOINTS

PART II. EFFECTS OF SURFACE ROUGHNESS, THE NATURE OF SURFACE ROUGHNESS, AND SURFACE AGING ON JOINT FRACTURE ENERGY

Robert O. Ebewele

Research Assistant
Materials Science Program, Engineering Research Building, Madison, WI 53706

Bryan H. River

Forest Products Technologist
Improved Adhesive Systems, U.S. Forest Products Laboratory,[1] Madison, WI 53705

and

James A. Koutsky

Professor of Chemical Engineering
Department of Chemical Engineering, University of Wisconsin, Madison, WI 53706

(Received 2 October 1979)

ABSTRACT

Tapered double cantilever beam specimens were used to test the effect of surface roughness, the nature of surface roughness, and surface aging on the fracture energy of phenolic-wood adhesive joints. The fracture energy and the failure characteristics of the joints were found to depend not only on the surface roughness but also on the method of surface preparation. The fracture energy increased monotonically with surface roughness for specimens derived from hand-sanded surfaces but exhibited a minimum for specimens obtained from machine-sanded surfaces. Generally, joints from hand-sanded surfaces had higher fracture energies than those derived from the machine-sanded surfaces. Within the joints derived from the machine-sanded surfaces, those sanded perpendicular to the direction of crack growth had higher fracture energies than those sanded parallel to the direction of crack growth. Aging surfaces prior to bonding significantly decreased adhesive joint strength.

Notwithstanding the differences in roughness, microscopic examination revealed little difference in the appearance of the sanded surfaces. Adhesive did not penetrate hand-sanded surfaces to any appreciable extent, but did deeply penetrate both the vessel and fiber lumens on the machine-sanded surfaces. Microscopic examination of the fractured surfaces did reveal significant differences that related to the fracture toughness of the bond.

Keywords: Tapered double cantilever beam, fracture energy, adhesive joints, phenol-resorcinol, surface roughness, adhesive penetration.

INTRODUCTION

Adhesion between two solid materials is generally small because, on an atomic scale, intimate contact between the surfaces of the materials is limited. This prevents the utilization of the available attractive surface forces. To overcome this limitation, liquid adhesive that has the capability of conforming to the solid

[1] Maintained at Madison, Wisconsin, in cooperation with the University of Wisconsin.

Wood and Fiber, 12(1), 1980, pp. 40–65

surface topography is introduced between the adherends. Therefore, the extent to which the adhesive conforms to the true surface determines the degree of success of the adhesion process. In addition, the strength of the surface and the strength of the adhesive are of utmost importance in determining bond quality.

Surface morphology influences the continuity of the wood-adhesive interface. The chemistry and absorbency of a surface can affect the adhesive cure. Although many have studied wood surface roughness and its effects on adhesive joint quality, it is still not well understood. Indeed there is neither a consensus on the definition of wood surface roughness nor how to measure it. Marian et al. (1958) considered a surface to be a composite of three levels of texture including (1) anatomic features, (2) machining features, and (3) errors of form. Stumbo (1960) defined surface roughness as the topography or irregularity of the interface between the substance and its surroundings, but he conceded that this definition is nebulous when applied to a porous substance such as wood. Stumbo's admission hints at one of the major problems that arises in assessing wood surface roughness in terms of its effect on adhesive bond quality. A wood surface is porous, permeable, and three-dimensional. Contact angle measurements and stylus tracings that suffice for many materials do not adequately characterize such a three-dimensional surface. Contact angles, for example, are influenced by penetration of the liquid into the surface. Stylus tracings may give the same reading for several widely different surfaces and do not detect what might be called the "internal roughness" of the surface.

Collett (1972) has provided a comprehensive summary and discussion of the research findings and viewpoints on the interfacial relationships between wood and other substances. Conclusions drawn by Collett from his review that are pertinent to the present study are:

1. Wettability seems to be of secondary importance in bond quality until wood density reaches or exceeds 0.80; thereafter wettability is of primary importance.
2. In theory roughness promotes adhesion, spreading, and penetration, all functions of "real" area.
3. Surface roughness of the right kind and amount is important to conventional wood-bonding adhesives that depend primarily on intermolecular forces for bonding.
4. Even though roughness promotes spreading, complete wetting of a rough surface is the exception not the rule and this leads to the formation of bondline voids.
5. Voids in a single plane are conducive to crack propagation; voids in variable planes are less detrimental to bond quality.

The present study is part of an overall program aimed at studying the effects of bonding variables upon bond strength and durability. In the first part of this series, we applied the techniques of fracture mechanics in the development of a tapered double cantilever beam (TDCB) specimen that we used to test the effects of bondline thickness, wood anisotropy, and cure time on the fracture energy of phenolic-wood adhesive joints. In this paper we report our findings on the effects of surface aging, surface roughness, and the nature of surface roughness on the fracture energy of adhesive joints.

ADHESIVE JOINT STRENGTH MEASUREMENT— THE FRACTURE MECHANICS APPROACH

The stress field in the vicinity of a crack tip can be adequately defined by the parameter K, the stress intensity factor. This parameter, a function of applied load and crack size, increases with load until, at a critical value $K = K_c$, a previously stationary or slow-moving crack propagates abruptly. This critical value, K_c, defines the fracture toughness. For adhesive joints, the analysis required to describe the stress field at the crack tip is extremely difficult. Consequently, fracture toughness is defined in terms of energy by exploiting the relationship between K and that of the strain energy release rate G. G is related to K by the equations:

$$G = \frac{K^2}{E}(1 - \nu^2) \text{ for plane strain}$$
$$G = \frac{K^2}{E} \qquad \text{for plane stress} \tag{1}$$

E = Young's modulus
ν = Poisson's ratio

G is a physical measure of the rate of release of strain energy at the crack tip.

For Mode I or opening mode where a cleavage stress field surrounds the crack tip, $K_c = K_{Ic}$, and hence $G_c = G_{Ic}$, Mostovoy et al. (1967), Mostovoy and Ripling (1971) and Ripling et al. (1963, 1964, 1971) have developed and applied the TDCB to a number of composite systems. We have adapted this for use in wood-based adhesive systems. Details of this were given in Part I of this series (Ebewele et al. 1979). Briefly, using the TDCB, fracture energy is given by the equation:

$$G_{Ic} = \frac{4P_c^2}{Eb^2}[m] \tag{2}$$

P_c = critical load necessary to cause a previously stationary or slow-moving crack to propagate abruptly
b = width of beam
m = a constant chosen so that beam compliance changes linearly with crack length (in this study m = 0.52 cm^{-1} (1.33 $inch^{-1}$) for all the specimens).
E = bending modulus of adherends

At P_c or K_c (G_c) the crack propagates until enough energy is lost to bring the crack to rest. The arrest load value given by P_a is related to fracture energy by the equation:

$$G_{Ia} = \frac{4P_a^2}{Eb^2}[m] \tag{3}$$

The condition of stable crack growth is defined when $P_c = P_a$ ($G_{Ic} = G_{Ia}$). The load-deflection profile is a continuous horizontal line in this situation. This is

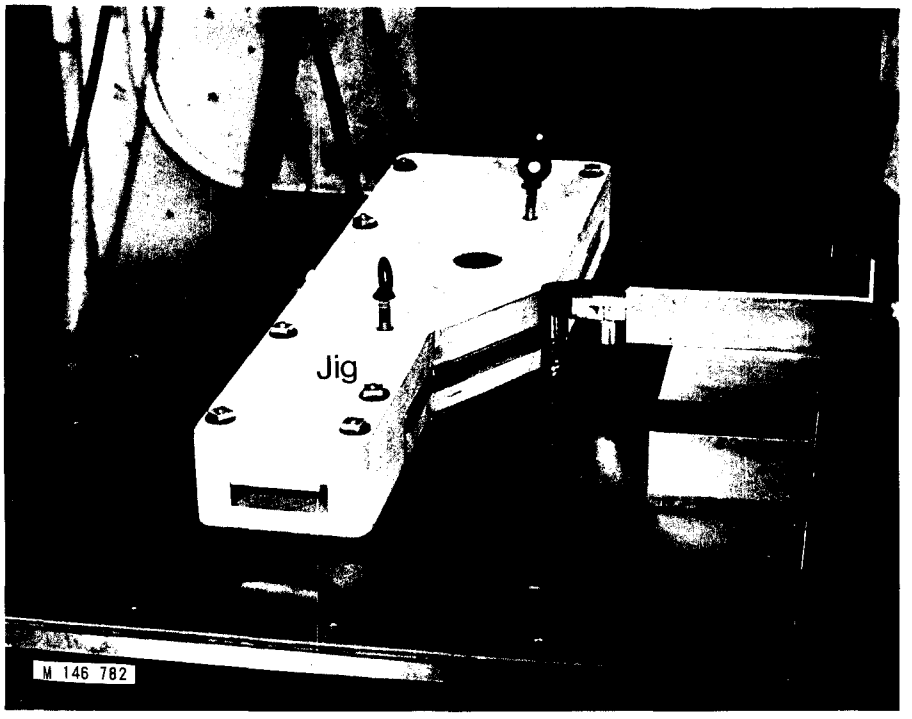

FIG. 1. Jig for positioning specimen during dimensioning with a high-speed router.

often the case with viscoelastic and ductile materials and weak interfaces. In contrast, brittle materials and strong interfaces with distinct initiation and arrest load values ($P_c \neq P_a$) result in a saw-toothed load-deflection profile.

EXPERIMENTAL

1. Specimen geometry

The TDCB developed and used for a number of composite systems by Mostovoy et al. (1967), Mostovoy and Ripling (1971), and Ripling et al. (1963, 1964, 1971) and adapted to wood bonding in our laboratories were used as test specimens. Details of the development of the test specimen were reported earlier (Ebewele et al. 1979).

2. Adherends

Hard maple (*Acer saccharum* Marsh) was chosen as the wood substrate because of its high modulus and uniform glue assimilation. Rough lumber for the specimens was conditioned to equilibrium at 23 C and 44% relative humidity (RH) (≅8% EMC). Generally, specimens were initially cut to their approximate dimensions, and had grain angles of 20° at the bonding surfaces. The surfaces to be bonded were sanded and finally cut to their appropriate dimensions ($m = 0.52$ cm^{-1}) using a special jig (Fig. 1).

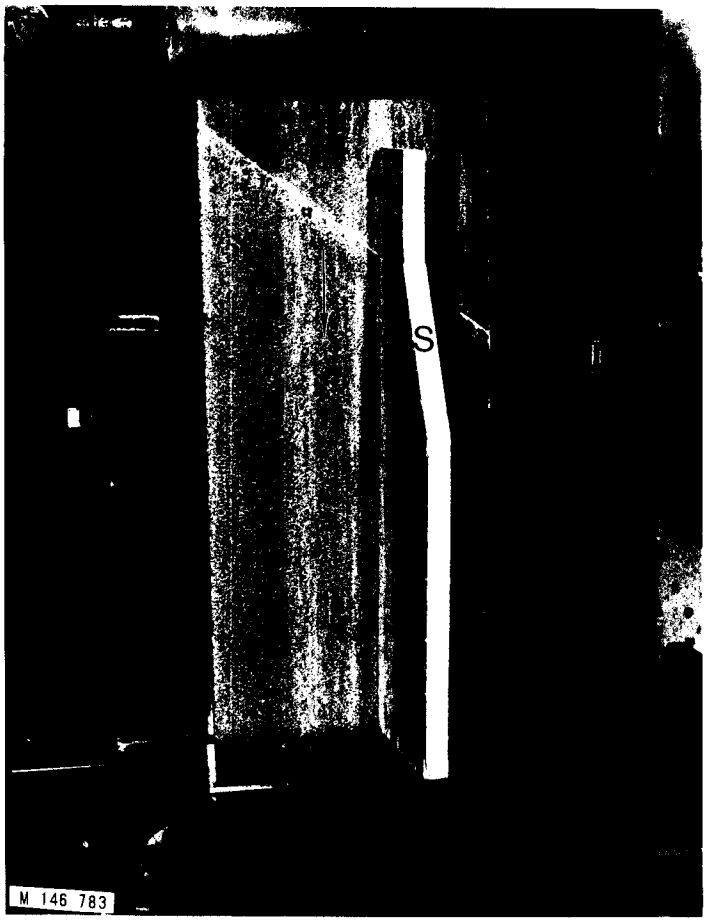
S
M 146 783

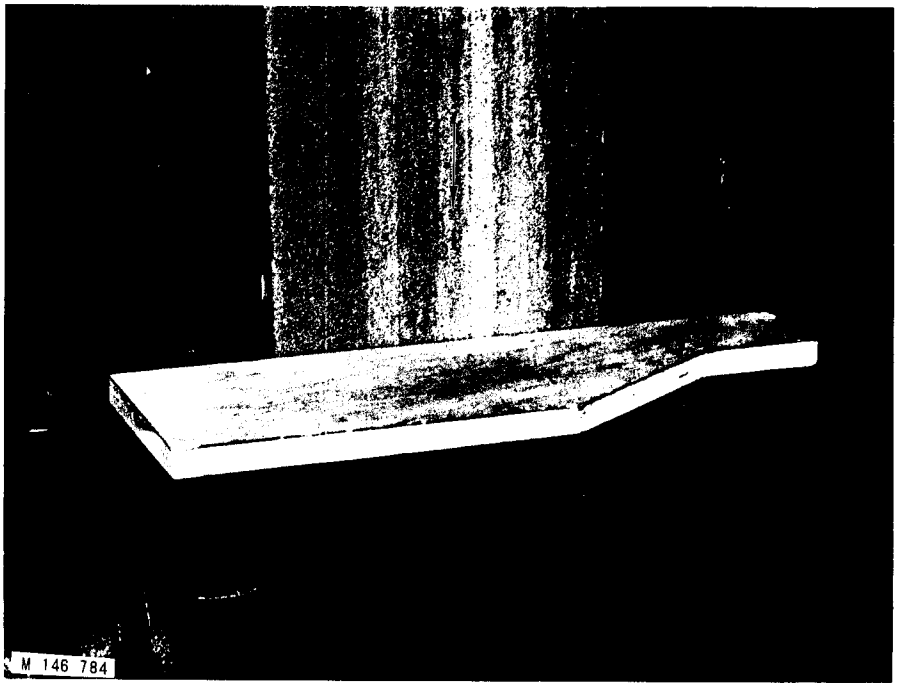
M 146 784

3. Abrasion techniques

The surfaces of the adherends to be bonded were sanded with one of the abrasive papers (Behr-Manning Co., Closekote Garnet Cloth Durabonded) grade 100, 80, 60, or 40. The first set of specimens was hand-sanded using reciprocating motion. A second set of specimens was machine-sanded perpendicular to the direction of crack growth. The surfaces in the last two sets were abraded parallel to the direction of crack growth with the belt moving in the direction of crack growth. The sanding procedure for the machine-sanded specimens is shown in Fig. 2. One set of specimens was jointed using the procedures outlined in Part I (Ebewele et al. 1979).

4. Surface roughness measurements

The surface roughness was measured perpendicular to the direction of abrasion. Measurements were made with a Micrometrical Instruments Company Profilometer Type PE. The profilometer is composed of amplimeter with tracer (Model 741), motortrace (Type V), and linkarms as shown in Fig. 3. The profilometer is activated by a stylus, which when traced over a surface, moves a coil in a magnetic field. The movement of the coil in the magnetic field produces a fluctuating voltage. The voltage produced depends on the height of the surface irregularities and the velocity at which the coil moves through the field, which in turn is dependent upon how fast the stylus is moved over the surface. The instrument includes a roughness width cutoff feature that is set to exclude features greater than a set width. A trace speed of 0.76 cm per second and a width cut-off of 0.76 mm were employed in this study. The profilometer reads out the height of irregularities directly in root-mean-square value.

5. Adhesives

A phenol-resorcinol resin, Koppers G4411A, was mixed with walnut shell flour-based hardener G4400B (containing 50% by weight paraformaldehyde) in the weight ratio of 100 gm resin to 20 gm hardener, i.e., 20 phr. The adhesive was mixed vigorously by hand for 10 min before spreading on the wood surfaces.

6. Bonding

Any debris on the sanded surfaces was removed by blasting the surface with compressed air passed through a 91-cm column of dry cotton cloth to remove any oil. Surface roughness was measured, and then the adhesive was carefully hand-brushed on both surfaces of the beams to be mated. For the unaged surfaces, the time between sanding and application of adhesive was within 2 h. For the aged specimens, after abrasion, surface roughness measurements and cleaning of surfaces, the beams were left in the conditioning room for between 3 and 4 weeks and then bonded. Open assembly times of about 1 min were used. Beams of about the same density were mated and a small mylar or teflon film of 2.54×10^{-2} mm (1 mil) thickness was inserted near the jaws of the specimens to provide

---

←

FIG. 2. Abrasion of specimen (S). Arrow indicates direction of movement of belt (B). A: Parallel abrasion. B: Perpendicular abrasion.

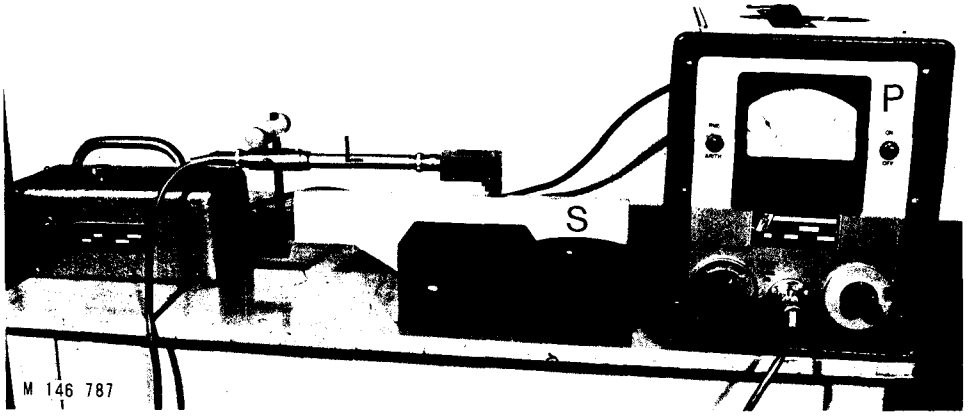

FIG. 3. Measurement of surface roughness with profilometer (P). The stylus on the linkarm (L) is moved across specimen surface (S) in a direction perpendicular to surface abrasion by the motor-trace (M).

the initial flaw. The specimens were placed in a press capable of holding two specimens simultaneously as shown in Fig. 4. The closed assembly time was 30 min. Glueline pressure (1.03–1.17 MPa, i.e., 150–170 lb/inch^2) was measured by a precalibrated compressometer. It was noted that for specimens cured for 5 h, the pressure decayed to zero by the time the specimens were removed from the oven because of the combined effects of metal expansion and wood drying. The resulting bondline thickness of specimens was in the range where fracture energy was independent of bondline thickness (Ebewele et al. 1979).

Before curing, excess glue was cleaned off the joint with a knife. The press with the samples was placed in a forced-air oven maintained at 70 C (±1 C). The bonding schedule is shown in Table 1.

7. *Fracture testing*

The progress of crack growth was monitored by shining a bright light on the rear of the specimen and making marks at the position of the emergent light after crack arrest. During testing, all lights in the room (except the one at the rear of

TABLE 1. *Bonding schedule.*

Set no.	Abrasion technique	Direction of abrasion with respect to crack growth	Aging	Cure time at 70 C
				H
I	Hand	Parallel	No	0.5
II	Machine	Perpendicular	Yes	5.0
III	Machine	Parallel	Yes	5.0
IV	Machine	Parallel	No	5.0

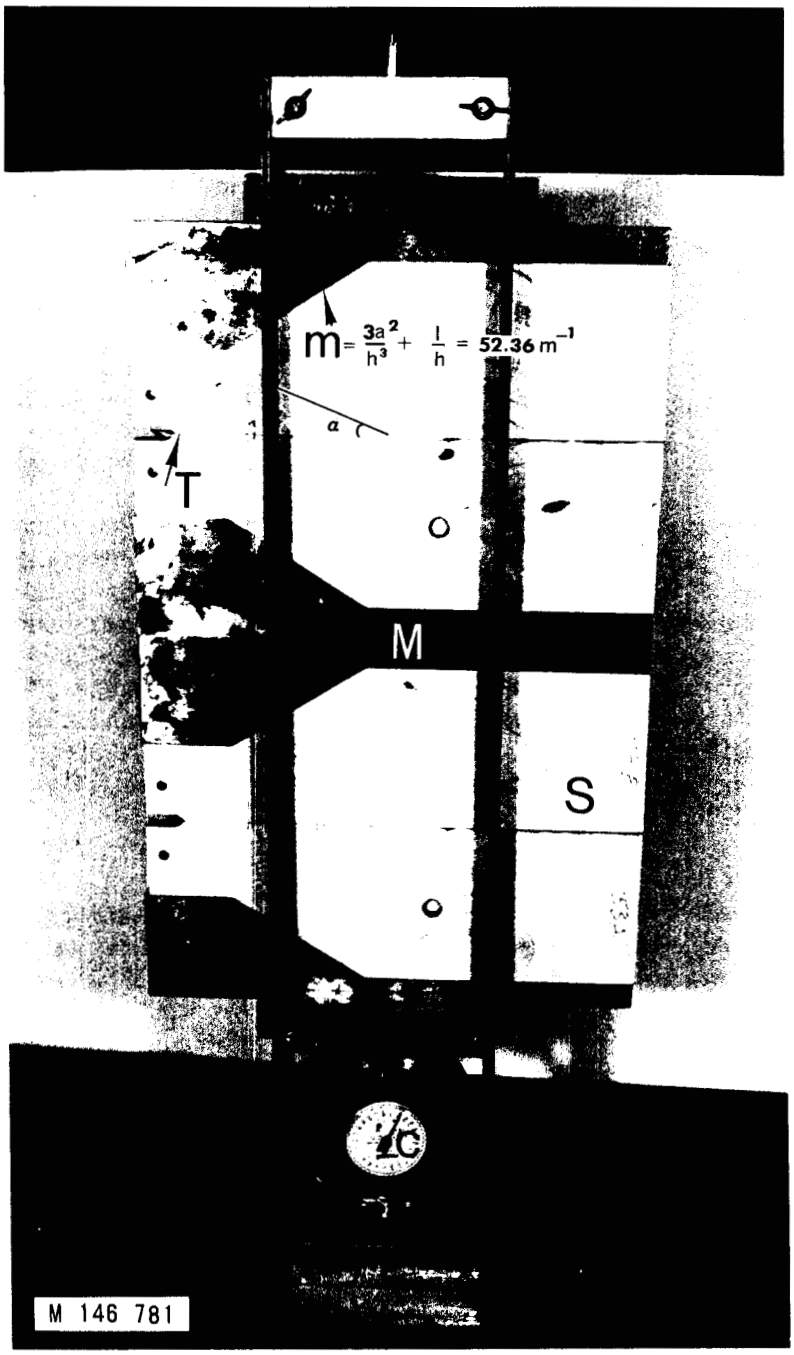

FIG. 4. Press for holding specimen (S) during care. Note the metal spacers (M) and teflon tape (T). Specimen contours M = 52.36 m^{-1}. Glueline pressure is read from a precalibrated compressometer (C). Press is capable of holding two specimens simultaneously.

the specimen) were shut off. Specimens were conditioned at 23 C, 44% RH for 3 days before cleavage fracture tests were carried out as shown in Fig. 5 on a Riehle (Ametek) Universal Testing Machine Model LDS-20. Sample deflections were measured by an LVDT (Daytronic Signal Conditioner Model 300D) mounted as shown in Fig. 5. Load and strain values were recorded on a Hewlett Packard HP-7004B X-Y recorder. A crosshead speed of 0.2 mm min^{-1} was used.

8. *Microscopy*

a. Scanning electron microscopy.—After fracture tests, the surface of the specimen on the edge opposite to the bonded surface was sanded by the same process used to prepare the original specimen. Microscopy specimens (10 mm × 5 mm × 2 mm) were cut from this freshly sanded surface. A Denton Vacuum Desk-1 Cold Sputter-Etch Unit was used for gold-shadowing the specimens at a pressure of 70×10^{-3} torr. Scanning electron micrographs were then taken using a Cambridge Scientific Instrument Stereoscan Mark 2A scanning electron microscope.

b. Fluorescence microscopy.—To determine the locus and type of failure, the fracture surface was examined by fluorescence microscopy utilizing ultraviolet (UV) radiation. In addition, serial sections (cross section and tangential oblique section) of the wood were examined to trace the depth and distribution of adhesive in the wood cells. The optical microscope employed was a Leitz Ortholux with mercury lamp having a UG-1 (Leitz) filter as the UV source. The natural bluish auto-fluorescence of the wood readily contrasted with the dark red/brown mass of the adhesive facilitating the identification of the location of the adhesive. The photomicrographs were taken with a 35-mm Kodak Plus-X Pan film (PX-135).

9. *Wettability measurements*

Generally wettability measurements are conducted by measuring the contact angle between a liquid and a surface. However, with a porous substance like wood, a substantial amount of any liquid suitable for these measurements is imbibed before a stable drop is formed. In our opinion, results from such measurements do not reflect the actual or dry surface condition of the wood. Instead they manifest the conditions of a liquid-modified or wet wood surface. In this study wettability was measured by the height to which the surface being tested was wetted by liquids of various surface tensions after 60 sec.

Twelve tapered beam adherends were selected at random from the failed fracture specimens for preparing wettability test specimens. Four 12-mm-wide strips were cut from each adherend. The strips were cut parallel to the fractured surface of the beam so that the same grain angle was maintained in the wetting specimens as was on the original bonded surface. Each set of four strips was assigned to either the hand-sanded or the machine-sanded group and to one of the six surface

→

FIG. 5. Fracture testing. A. Test machine (Riehle Ametek). Testing machine with Daytronic Signal Conditioner (D) and Hewlett Packard X-Y Recorder (R). B. Closeup of specimen (S) with grips (G), load cell (C), and rear light (L). Note position of LVDT.


R
L
S
D
M 146 785

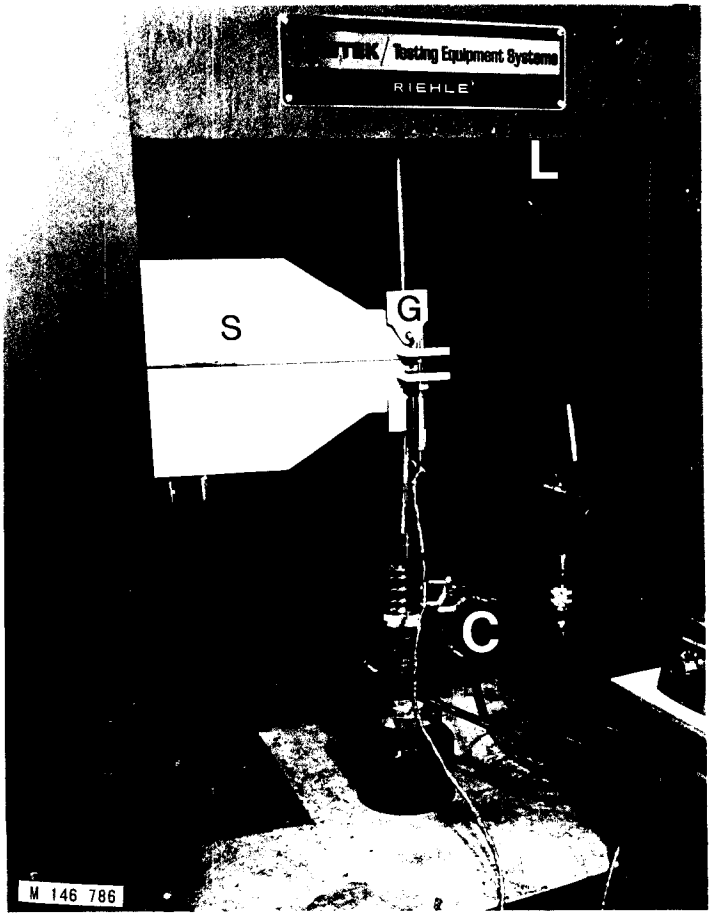
TTBK / Testing Equipment Systems
RIEHLE
L
S
G
C
M 146 786

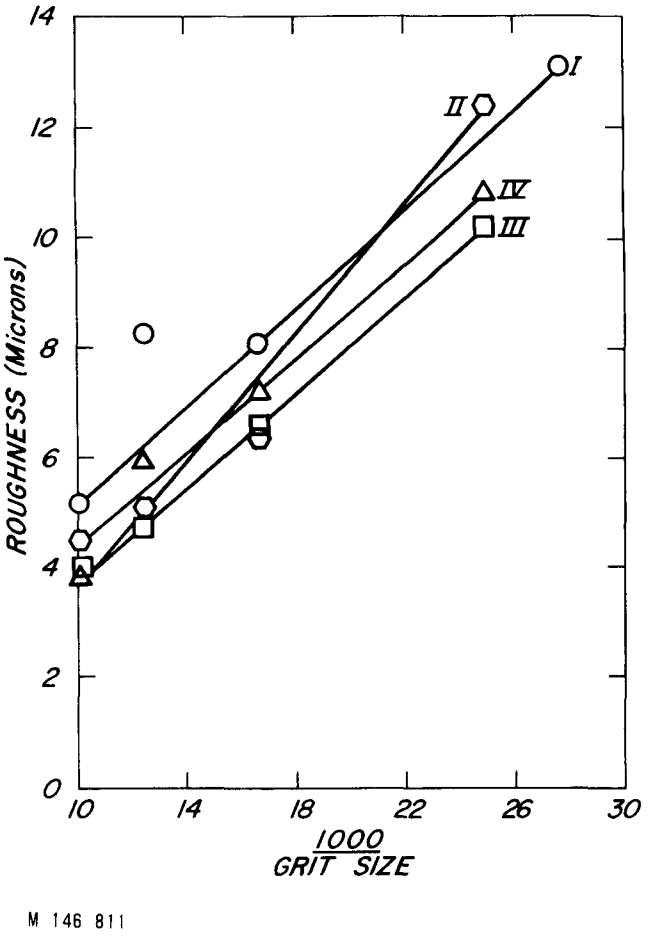

FIG. 6. Roughness of hand- and machine-sanded surfaces of hard maple obtained with abrasive papers of grade number ranging from 36 to 100.

tensions. Each strip in each set was further assigned to one of the four grit sizes. Thus, all the strips for a given method of sanding and surface tension were from the same piece of wood and the effects of grit size on wetting could be readily evaluated.

A test specimen 12 mm × 12 mm × 150 mm was cut from each strip. The 150-mm dimension was parallel to the fractured surface. Each specimen had two opposite surfaces with the grain angle to the surface matching the angle to the bonded surface in the original beam (20°). One such surface of each specimen was then prepared by the sanding method and grit size to which it was assigned. Surfaces were sanded parallel to the long dimensions (direction of crack propagation). The freshly sanded surface was blasted with cleaned compressed air to remove excess sanding debris. Wettability measurements were made immediately after surface preparation.

Liquids of six different surface tensions were prepared from various concentrations of formamide in water. Two milliliters of each of these liquids were

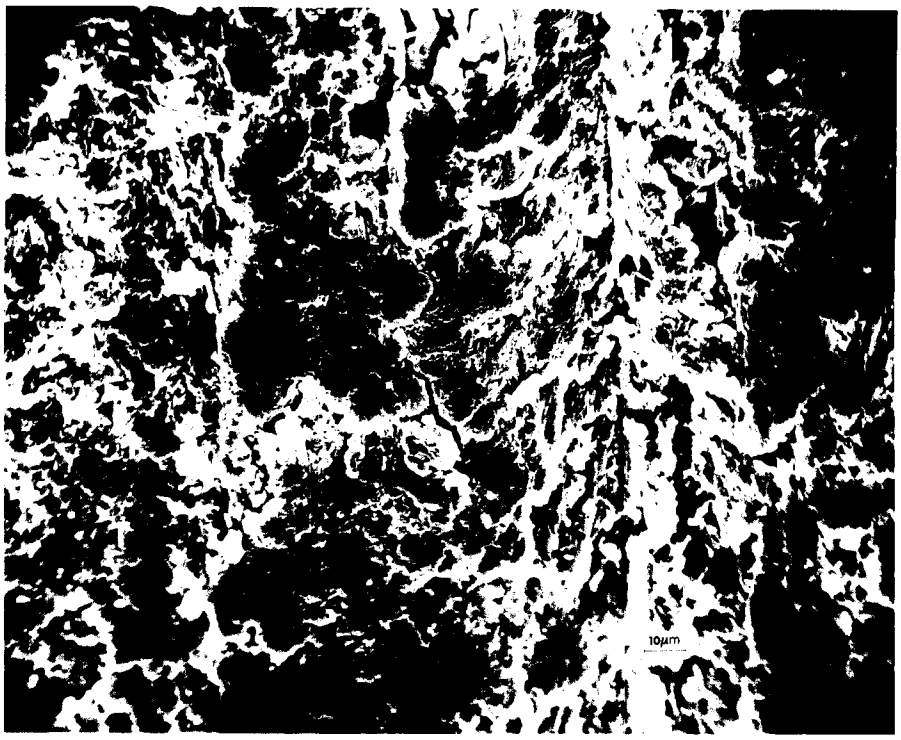

FIG. 7. Hard maple surface prepared by hand-sanding with abrasive paper grade number 80.

measured into a graduated cylinder. Each specimen was carefully lowered into its cylinder to avoid any splashing of the liquid in the cylinder. The level of the liquid immediately after lowering the wood sample into the cylinder was recorded. Then after 1 min, the height of the sanded surface wetted by the rising liquid was marked off, and the difference between the readings was recorded. The sample

TABLE 2. *Wettability measurements*[a] *of sanded maple surfaces.*

Abrasive paper grade number	Surface tension of liquid					
	58.7	59.3	62.3	65.1	66.5	6.94
	Dyn/cm					
Hand-sanded surfaces						
100	14	10	10	12	12	10
80	14	13	16	19	16	12
60	13	10	12	19	14	9
36	16	19	18	20	22	23
Machine-sanded surfaces						
100	12	18	20	27	22	4
80	16	22	18	18	28	16
60	14	21	20	22	26	5
40	12	29	22	28	29	13

[a] Distance (mm) wetted in 1 min.

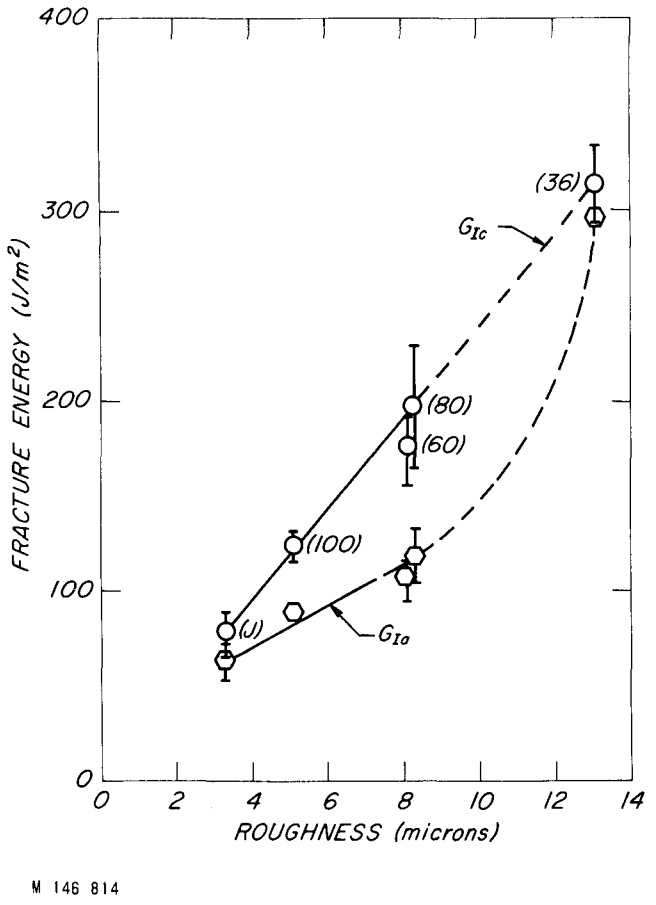

FIG. 8. Variation of fraction initiation energy (G_{Ic}) and fracture arrest energy (G_{Ia}) with surface roughness for specimens derived from hand-sanded surfaces (SET I). The numbers in parentheses represent the abrasive paper grade number and J indicates data for jointed surfaces. Note that as roughness increased, the difference $\Delta G_{Ic} = G_{Ic} - G_{Ia}$ increased except for the 36 grit specimens where $G_{Ic} \cong G_{Ia}$.

was oriented with the sanded, 20° grain angle surface perpendicular to the liquid surface and with the grain angle tilted upward to avoid capillary rise of the liquid through the cell lumens to the sanded surface.

RESULTS

The results are shown in Figs. 6 through 16 and in Table 2. Each data point in Figs. 6, 8, 11, 12, 13, and 14 represent two specimens and each specimen produced at least three measurements of the fracture initiation energy G_{Ic}, and the fracture arrest energy G_{Ia}. The numbers in parentheses on the graphs indicate the abrasive paper grit size, and (J) indicates data for knife-jointed surfaces. Micrographs were selected to be as nearly representative of the overall appearance of a given surface as possible.

FIG. 9. Photomicrograph of the adhesive layer and one hand-sanded adherend showing lack of adhesive penetration of vessels and fibers.

The roughness of sanded surfaces increased linearly with the abrasive grit size (Fig. 6). Notwithstanding the difference in roughness, microscopic examination revealed little difference in the appearance of the surfaces. Cell structure was destroyed by the sanding treatments. The surfaces all had the appearance of having been smeared (Fig. 7). Hand-sanded surfaces were less absorbent of liquid than machine-sanded surfaces but within a given sanding process, coarser grit produced more absorbent surfaces (Table 2).

The fracture initiation energy, G_{Ic}, and the fracture arrest energy, G_{Ia}, of hand-sanded specimens increased with roughness (Fig. 8). Generally, the adhesive did not penetrate the hand-sanded surfaces to any great extent (Fig. 9). The fractured surface showed wood failure, which increased in depth and roughness as roughness of the surfaces from which the specimens were initially derived increased (Fig. 10). The extent of wood failure in the 36 grit specimens was such that failure characteristics were indicative of stable crack propagation in contrast to the unstable crack growth exhibited by specimens prepared from finer grit papers. Thus for the 36 grit specimens $G_{Ic} \cong G_{Ia}$. However, in all cases the wood failure was shallow. Relative to the fractured surfaces of the machine-sanded specimens, the fractured surfaces of the hand-sanded specimens were quite rough. Microscopic examination revealed that the roughness was caused by the crack front passing repeatedly back and forth across the glueline from one adherend to the other as shown schematically in Fig. 18A.

In contrast to the behavior of hand-sanded specimens, the fracture energies of machine-sanded specimens first decreased then increased with the increasing roughness of the sanded surface (Figs. 11–13). Adhesive deeply penetrated both

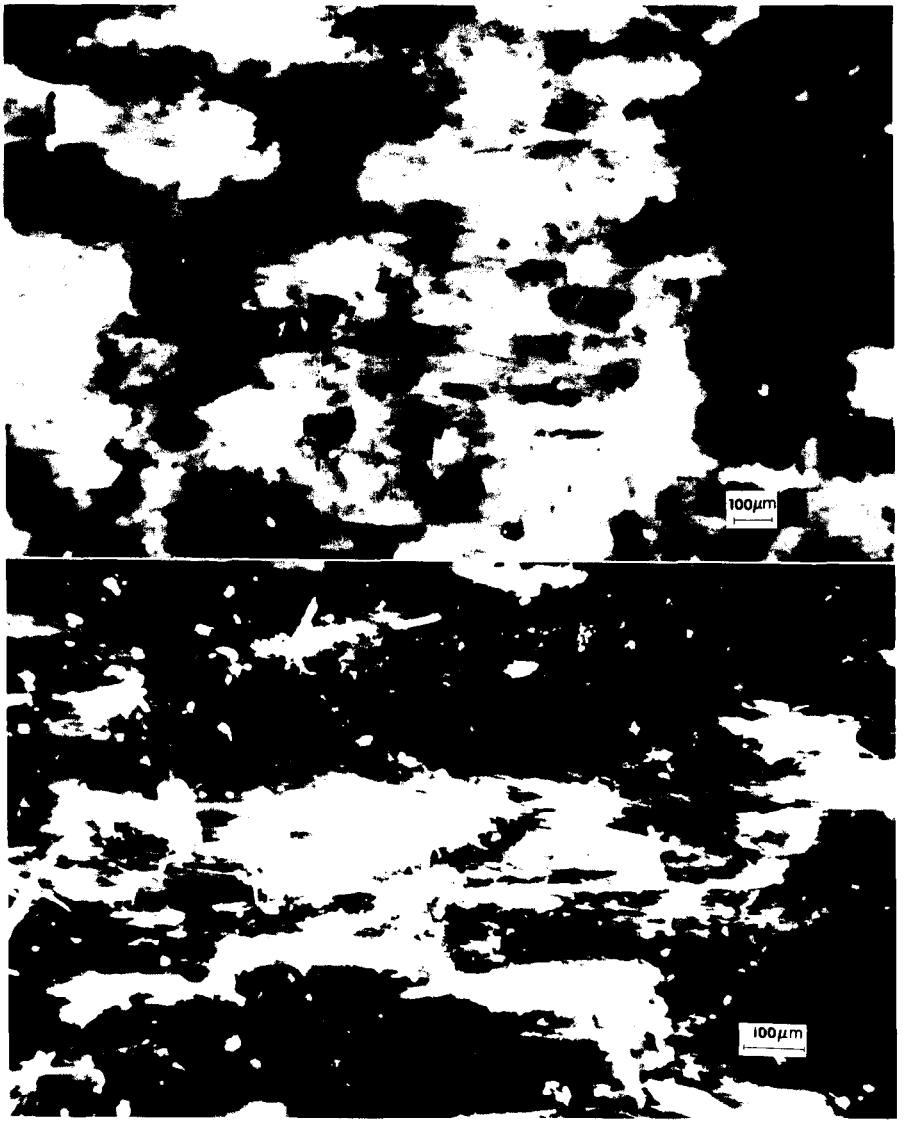

FIG. 10. Photomicrographs of fractured surfaces of specimens prepared from hand-sanded surfaces. Fractured surface of specimen derived from 100 grit abraded surface (top photo) shows fuzzy indistinct and very shallow wood failure. Note light areas are wood, dark areas are adhesive. Fractured surface of specimen derived from 36 grit abraded surface (bottom photo) shows distinct, deeper and torn wood failure.

the vessel and fiber lumens on the machine-sanded surfaces (Fig. 15). Little or no wood failure was evident on the fractured surfaces. The crack passed continuously through the glueline, accounting for the smoother appearance of the fracture surfaces compared to those of hand-sanded specimens (Fig. 16). The path of the crack for machine-sanded specimens is shown schematically in Fig. 18B.

Fracture energies of specimens machine sanded perpendicular to the direction of crack propagation were higher than the energies of specimens sanded parallel

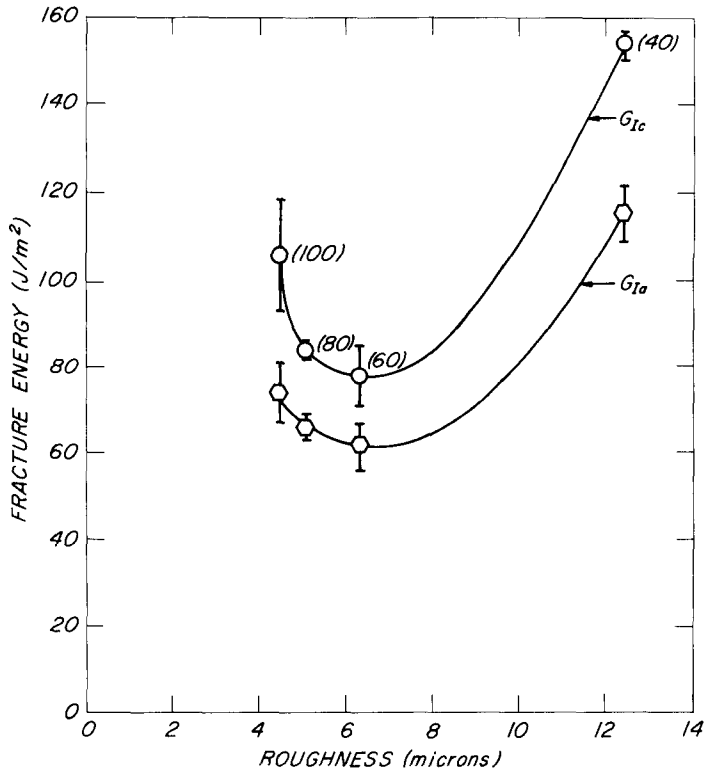

FIG. 11. Variation of fracture energies (G_{Ic} and G_{Ia}) with surface roughness. The specimens were derived from surfaces machine-sanded perpendicular to the direction of crack growth (SET II). Surfaces were aged 3 to 4 weeks at 73 F (23 C), 44% RH before bonding. Observe a minimum in the fracture energy-surface roughness profile at the 60 grit specimens.

to the crack direction (Figs. 11 and 12). Machine-sanded surfaces, which were aged before bonding, resulted in lower fracture energies than surfaces bonded quickly after sanding (Figs. 12 and 13).

Figure 14 compares the fracture initiation energies, G_{Ic}, of the various bonding schedules as a function of surface roughness. Observe that at the same roughness value, specimens derived from hand-sanded surfaces have much higher fracture energies than those derived from machine-sanded specimens, especially for rougher surfaces. This is particularly intriguing when one recalls that these specimens were cured for only one-half hour. Previous work in our laboratories (Ebewele et al. 1979) showed that fracture energy increases considerably with cure time.

The difference between the fracture initiation energy and the fracture arrest energy, $G_{Ic} - G_{Ia} = \Delta G_{Ic}$, is a measure of the brittleness of the system. For an ideally brittle system, i.e., one that offers little or no resistance to crack propagation, once the energy stored in the system reaches the critical value necessary for crack propagation, the system fails catastrophically and all the energy stored

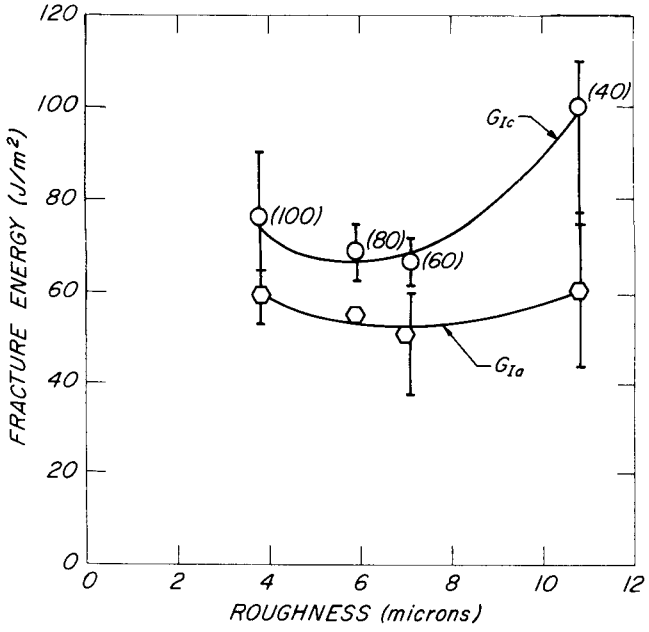

M 146 816

FIG. 12. The fracture energies of specimens prepared by machine-sanding parallel to the grain with 100, 80, 60, and 40 grit abrasive papers. Surfaces were bonded within 2 hours of sanding.

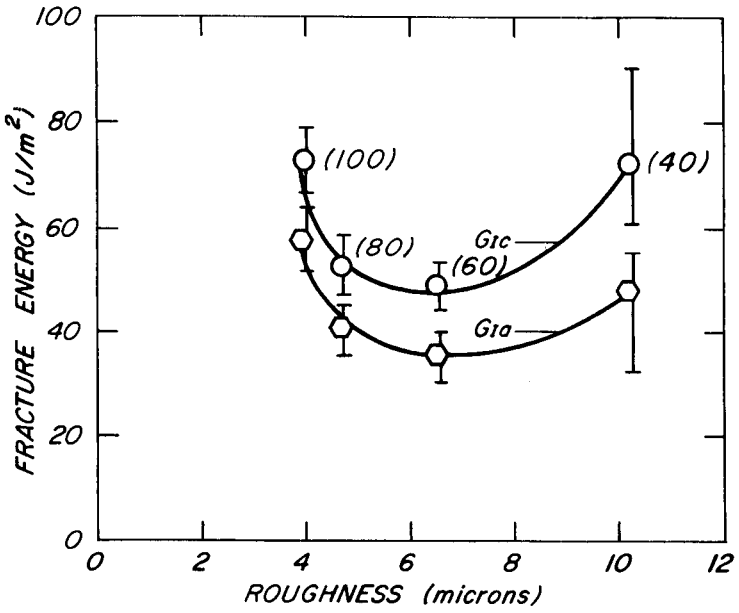

M 146 809

FIG. 13. The fracture energies of specimens derived from surfaces machine-sanded parallel to the grain with 100, 80, 60, and 40 grit papers. Sanded surfaces were aged 3 to 4 weeks at 73 F (23 C), 44% RH before bonding.

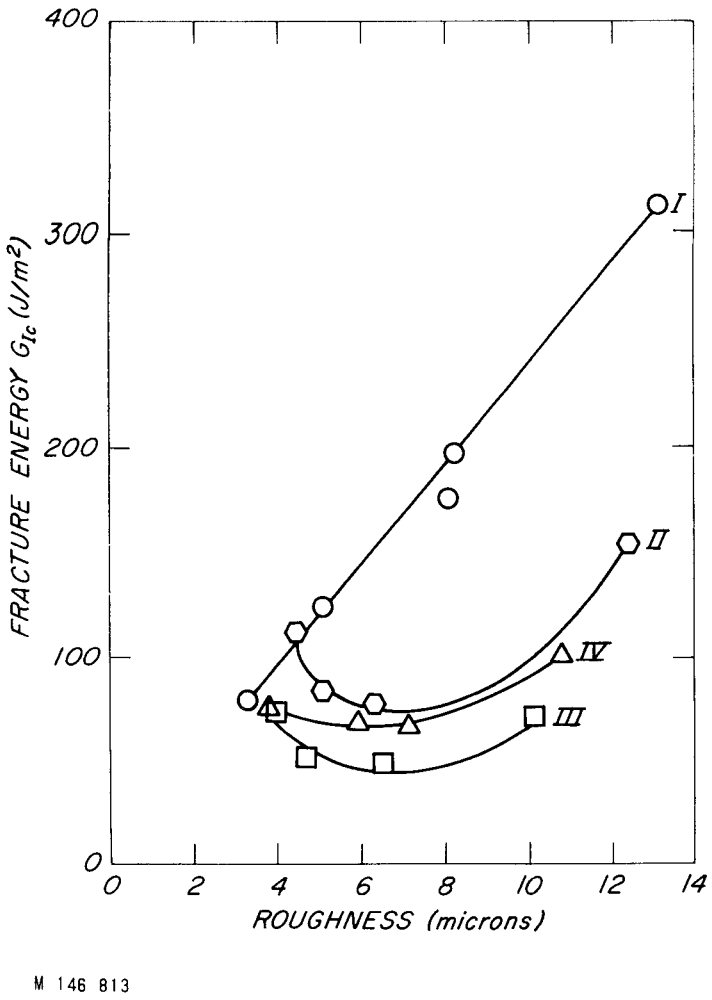

FIG. 14. Relative fracture initiation energies, G_{Ic}, for the various surface treatments. Note that the trend in fracture energy is in the order: hand-sanded (SET I) > machine-sanded (SETS II, III, IV). Within the machine-sanded surfaces, the order of fracture energy is: perpendicular abraded surfaces (SET II) > unaged parallel – abraded surfaces (SET IV) > aged parallel – abraded surfaces (SET III).

in the system is dissipated. However, for ductile or viscoelastic systems, catastrophic failure is prevented by plastic deformation, which blunts and arrests a propagating crack. In Figs. 8, and 11 through 13, ΔG_{Ic} or brittleness of the system increased with increasing fracture energy (G_{IC}). This was especially notable at greater roughness except for the 36-grit hand-sanded specimens where pronounced wood failure occurred. By implication and from Fig. 14, the susceptibility to brittle failure of adhesive joints derived from surface abrasion of adherends is in the order: Hand-sanded > machine-sanded and within machine-sanded systems: perpendicular abraded > unaged surfaces > aged surfaces.

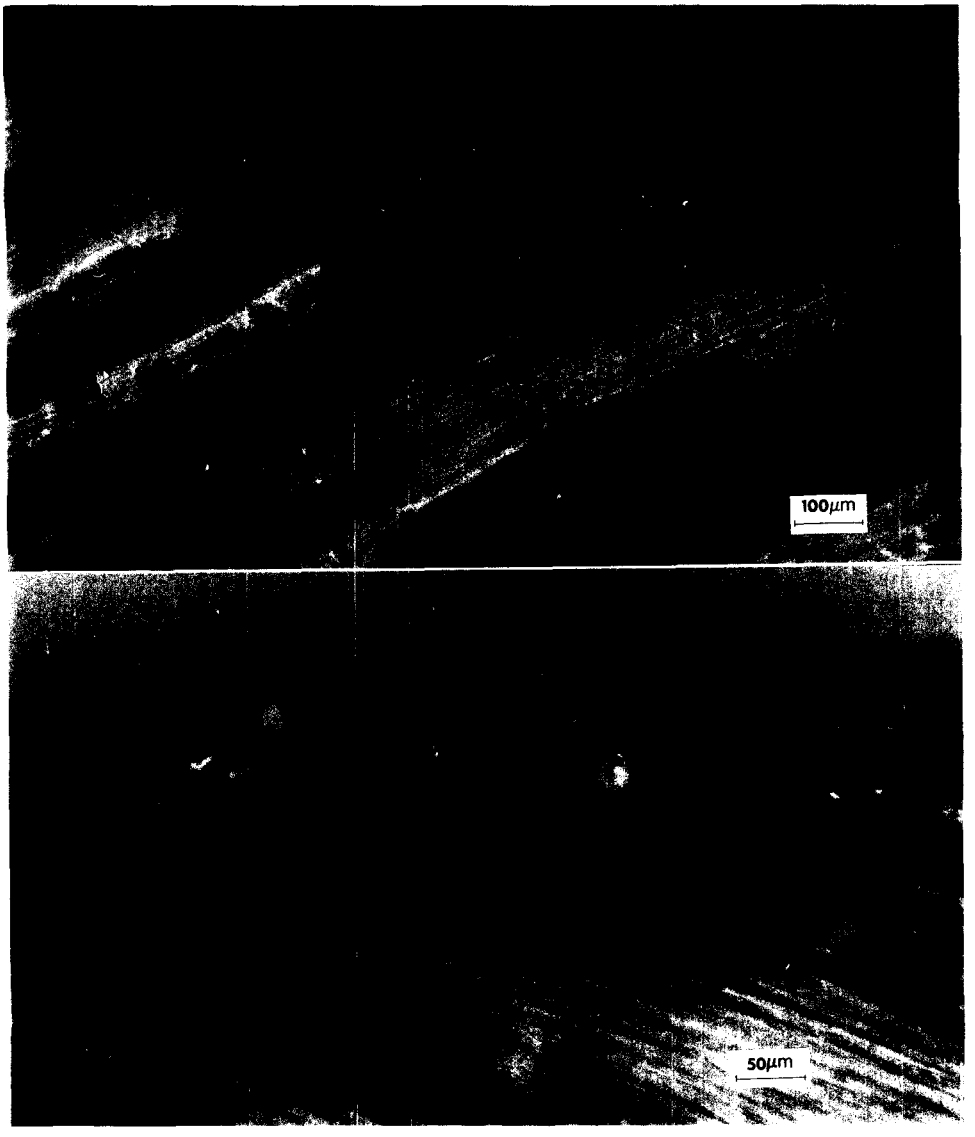

FIG. 15. Photomicrographs of the side of a machine-sanded specimen showing penetration of vessels (top) and fibers (bottom).

DISCUSSION

Roughness of surfaces prepared with different grit sizes did not vary greatly between the hand and machine methods of surface preparation, yet the fracture energy-roughness relationship of hand-sanded specimens differed significantly from the relationship in machine-sanded specimens. Striking differences between specimens prepared by the two different processes were also observed in the nature of the joint and its failure. The differences are shown in Table 3.

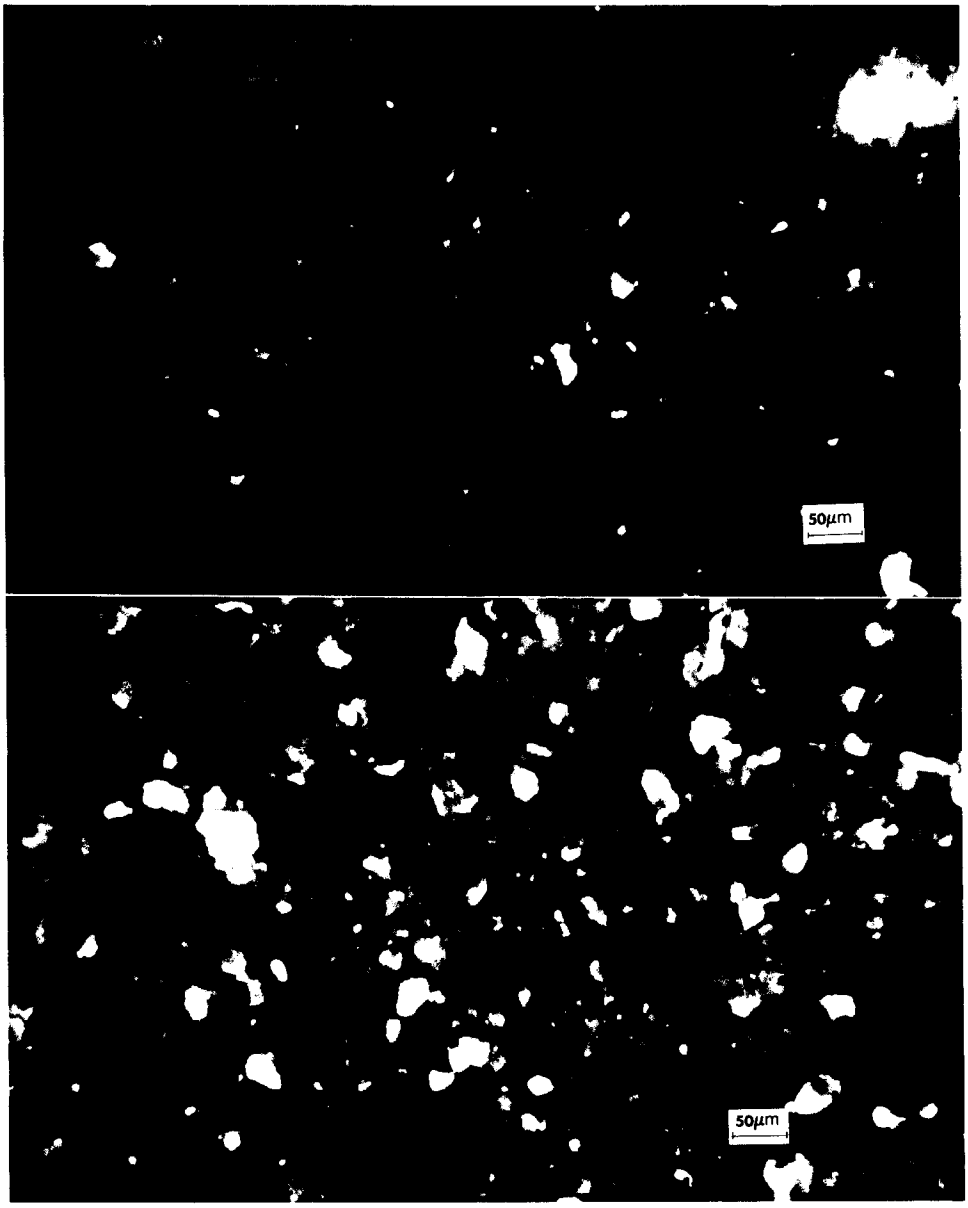

FIG. 16. Photomicrographs of adjacent fracture surfaces of a specimen prepared from machine-sanded surfaces showing the crack to be near but not entering the surface of one adherend (top) and at the surface of a zone of adhesive layer with high filler concentration (bottom). Adhesion failure to the filler particles (white areas) appears likely.

We think that the trend in fracture energies obtained with both the hand-sanded and machine-sanded surfaces indicates the operation of the "Cook-Gordon crack stopping or delamination-induced strengthening mechanism" (Cook and Gordon 1964). Briefly, under plane strain conditions, a triaxial tensile stress state is de-

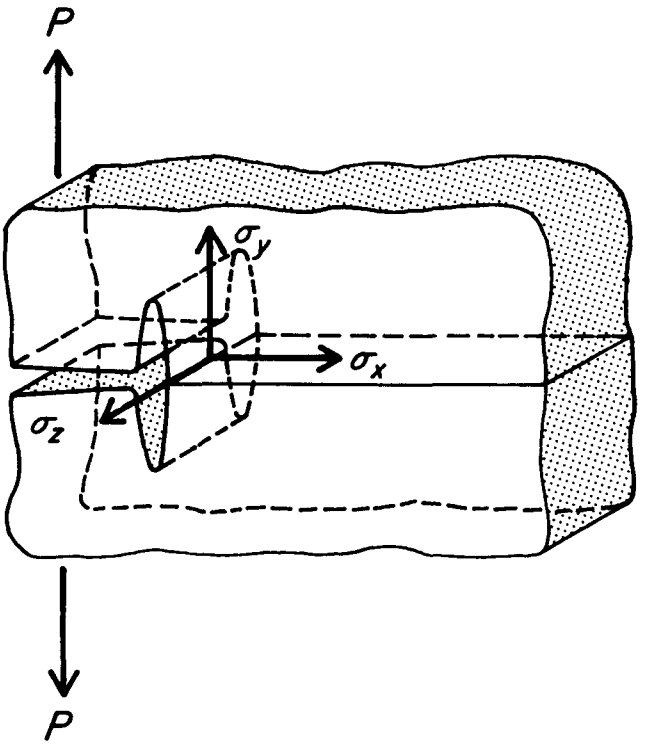

FIG. 17. Blown-up view of crack front showing the triaxial distribution of stresses at the crack tip. For weak interfaces placed perpendicular to the direction of crack growth σ_x can cause delamination ahead of the crack front. Similarly σ_z can cause delamination of weak interfaces placed perpendicular to the crack front. In either case, σ_x or σ_z is reduced to zero at the free surface thus reducing triaxiality.

veloped at the crack tip. Since fracture toughness is known to increase with decreasing triaxility, improved toughness can be obtained if the crack-tip-induced σ_x and/or σ_z stresses (Fig. 17) can be reduced. Since no stresses exist normal to a free surface, σ_x can be reduced to zero by generating an internally free surface normal to the direction of crack growth. That is, moderately weak interfaces placed perpendicular to the crack growth direction can be readily pulled apart ahead of the crack front by the σ_x stresses, which are consequently reduced to zero. In addition, the crack is blunted by the free surface further reducing triaxiality. Both of these conditions improve fracture energy. Similarly delamination of interfaces normal to the thickness direction (z) not only reduces σ_z to zero at each delamination but also decreases the effective thickness of the sample. The net result is a reduction of triaxiality. Consequently, the specimen behaves like a series of thin-plane stress samples instead of one thick-plane strain sample.

In wood, the weak interfaces are the bonds between the radial and tangential surfaces of the cells. For the hand-sanded surfaces, we claim that sanding against the grain, as in the back-and-forth motion of the hand during hand-sanding, prefailed the weak interfaces between the cells as represented in Fig. 19B. McKenzie

TABLE 3. *A comparison of differences in the features of bondlines and bondline fractures of specimens prepared with hand- or machine-sanded surfaces.*

Hand-sanded	Machine-sanded
1. Wood failure—shallow but extensive, increasing in amount and depth as grit size increased.	1. Wood failure—none or a very slight amount in the 40 grit specimens.
2. Crack path—devious traveling repeatedly back and forth from one adherend to the other, not traveling forward through the adhesive in a straight line for any distance (Fig. 18).	2. Crack path—follows a relatively straight line, never leaving the adhesive layer, may wander gradually to the opposite adherend. Path follows a very thin line between the wood surface and the filler rich central portion of the bondline (Figs. 16 and 18).
3. Adhesive penetration—none or shallow and sparse.	3. Adhesive penetration—extensive and deep leaving filler particles behind in the glueline proper (Fig. 15).
4. Adhesive layer thickness—thick, about 0.008 inch.	4. Adhesive layer thickness—thin, about 0.0004 inch.

(1960) has demonstrated the failure of the weak interfaces between the cells during machining perpendicular to the grain. Such prefailure effectively reduces σ_x to zero and blunts the crack, both of which increase fracture energy. The operation of this mechanism can be seen in the splintered bending failure of wood. In an earlier report, we presented evidence that suggested that this crack-stopping mechanism is still operative although less effective when the weak interfaces are at angles less than 90° to the path of the crack. In the present study the orientation of the grain with respect to the bonded surfaces of the adherends was 20°. This grain orientation happened to yield the lowest fracture energy in the previous study with values of about 25 J/m^2. It is apparent from fracture energies of hand-sanded specimens that the effectiveness of the delamination-induced strengthening is increased by coarser grit sizes, which no doubt fail the weak interfaces to a greater depth than fine grit sizes. The fact that adhesive did not significantly penetrate the surface may have ensured the effectiveness of the weak interface crack-stopping mechanism. Had the adhesive penetrated, it would have "healed" the prefailed interfaces resulting in a performance similar to the machine-planed specimen in the previous study and the machine-sanded specimens in the present study.

During machine sanding, the ends of the cells were brushed smoothly in the direction they were pointing by the grit as shown in Fig. 18A. In this process there was less tendency to prefail the weak interfaces between the cells or to fill the cell lumens with sanding debris. During gluing, the adhesive successfully penetrated the machine-sanded surface and after cure formed a tough interpenetrated, three-dimensional layer at the wood surface. In this reinforced layer, the prefailed weak interfaces, if present, would be rebonded and their failure under load less probable, thus reducing the effectiveness of this crack-stopping

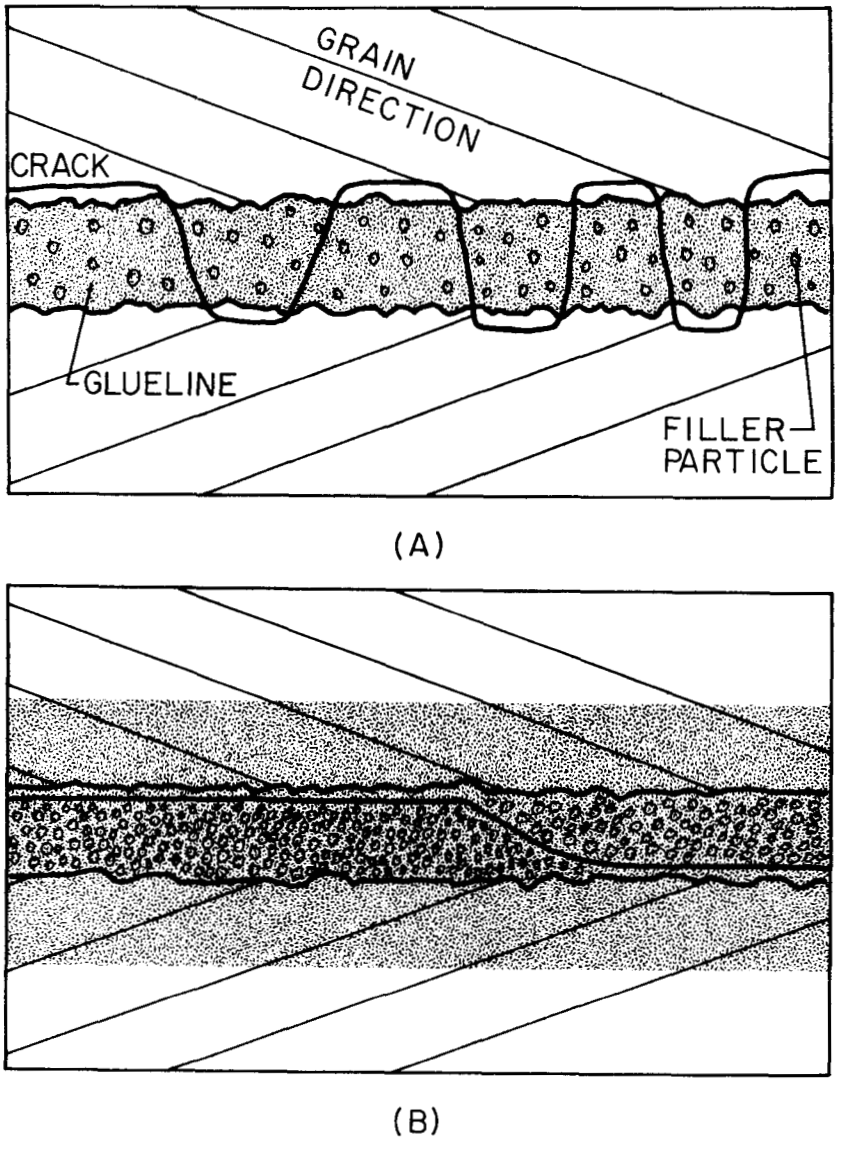

FIG. 18. Schematic diagram of the difference in adhesive penetration filler concentration and the path of the crack in hand-sanded specimens (A) and in machine-sanded specimens (B).

mechanism. At the same time, the loss of adhesive from the adhesive layer due to the penetration reduced the layer thickness to about one-half that in hand-sanded specimens. Curiously, when the adhesive penetrated the wood it did not carry the walnut shell flour particles along, in spite of the fact that the particle diameters were smaller than the vessel lumens. This phenomenon has been noticed by at least one other researcher (DeRiberolles 1958). Its effect was to concentrate the filler in the adhesive layer. During failure of the machine-sanded

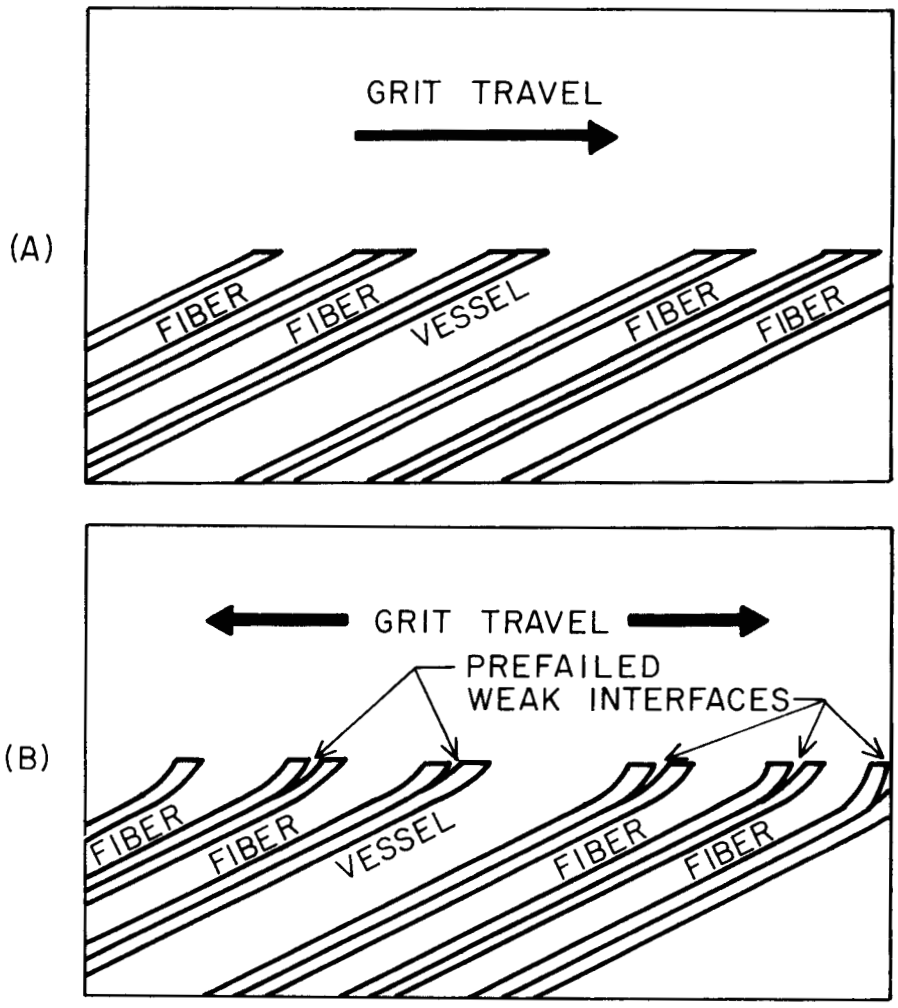

FIG. 19. Schematic diagram of the effects of machine-sanding versus hand-sanding on the exposed ends of the wood fibers and vessels.

specimens, the crack generally followed a narrow path between the two highly interpenetrated layers, i.e., wood-adhesive and filler-adhesive. More specifically crack growth seems to have occurred by failure in adhesion to filler particles at the outer limit of the filler-adhesive layer. The evidence is shown in Fig. 16 where in the upper photomicrograph the failed surface consists of the adhesive-penetrated wood. Little wood failure, indicated by light areas, is evident. The opposing fracture surface in the lower photomicrograph shows a large number of white particles which are walnut shell flour. Gray particles are walnut shell flour embedded in the adhesive below the fracture surface.

For the machine-sanded specimens, the fracture energy-roughness profile may also involve operation of the Cook-Gordon crack-stopping mechanism. However,

in this case, the locus of delamination has changed from prefailed wood surface in the hand-sanded specimens to the adhesive-filler interface. Presumably, fillers were aligned in the well-defined series of valleys created on the surfaces by machine-sanding. For surfaces sanded perpendicular to the direction of crack growth, these valleys represent weak interfaces which could easily be pulled apart by the induced σ_x stress which is itself consequently reduced to zero. In other words, perpendicular abrasion creates surfaces which effectively act as "crack arresters."

On the other hand, the valleys from parallel abrasion constitute weak interfaces which can be delaminated thus reducing σ_z to zero. In this case, parallel abrasion results in surfaces that act as effective "crack dividers." If this is the case, one would expect the fracture energy to decrease continuously with decreasing number of valleys (i.e., decrease with increasing grit size). However, with the 40 grit specimens, minute wood failure occurred. This suggests the operation of a crack-stopping mechanism akin to that operative in the hand-sanded specimens. Since the fracture energies of hand-sanded specimens were generally higher than those of machine-sanded specimens, the energy of the 40 grit machine-sanded specimens would be expected to be close to that obtained in the hand-sanded specimens.

The above explanation of the trend of fracture energy with respect to roughness is one possible explanation. We do not exclude the possibility of other explanations. The fracture energy-roughness relationship shown may be caused by an interaction between competing variables. For example, in the previous study, there was evidence that the fracture energy is very sensitive to the thickness of the adhesive layer between 0.003 and 0.004 inch. The machine-sanded specimens had bondlines in this thickness range, so it may be possible that the effective bondline thickness changed with grit size (roughness) and thus influenced the fracture energy.

CONCLUSIONS

1. The fracture toughness of an adhesive joint depends on the surface texture of the adherends and on the method of surface preparation.
2. Adhesive joints between reciprocally hand-sanded surfaces had different fracture mechanisms and higher fracture energies than those from unidirectionally machine-sanded or jointed surfaces.
3. The highest fracture energies with machine-sanded surfaces were obtained by sanding perpendicular to the direction of crack growth (perpendicular to the grain).
4. Surfaces prepared with coarser grit sizes in both hand- and machine-sanding produced higher fracture energies than those prepared with finer grit sizes in the range between 40 to 100 grit.
5. Freshly prepared surfaces, machine-sanded parallel to the direction of crack propagation produced higher fracture energies than similar surfaces aged 3 to 4 weeks at ambient conditions before bonding.
6. The tapered double cantilever beam specimen (TDCB) is sensitive to differences in fracture behavior revealed by microscopic examination of failed surfaces.

7. Further research will be necessary to fully explain the relationships revealed by this study.

ACKNOWLEDGMENT

We wish to thank the Weyerhaeuser Corporation and the Forest Products Laboratory (Forest Service, U.S. Department of Agriculture) in Madison for providing generous support for this research. We would like, in particular, to thank Dr. Roland Kreibich of Weyerhaeuser for his helpful advice and critical comments during the course of this investigation.

We also wish to thank Dr. Lidija Murmanis and Dr. Irving Sachs of the Forest Products Laboratory for helping with microscopy. In addition we would like to thank Dr. George Myers, Dr. Alfred Christiansen, and Dr. Joseph Murphy of the Forest Products Laboratory for their useful suggestions.

REFERENCES

COLLETT, B. M. 1972. A review of surface and interfacial adhesion in wood science and related fields. Wood Sci. Tech. 6:1–42.

COOK, J., AND J. E. GORDON. 1964. A mechanism for the control of crack propagation in all-brittle systems. Proc. R. Soc. of London 283(1391):508–520.

DERIBEROLLES, J. P. 1958. The influence of surface texture on the strength of butt-end glued wood. University of California, For. Prod. Lab., Richmond, Calif. (M.S. Thesis).

EBEWELE, R. O., B. H. RIVER, AND J. A. KOUTSKY. 1979. Tapered double cantilever beam fracture test of phenolic-wood adhesive joints. Part I. Wood Fiber 11(3):197–213.

MARIAN, J. E., D. A. STUMBO, C. W. MAXEY. 1958. Surface texture of wood as related to glue-joint strength. For. Prod. J. 8(12):345–351.

MCKENZIE, W. M. 1960. Fundamental aspects of the wood cutting process. For. Prod. J. 10(9):447–456.

MOSTOVOY, S., P. B. CROSLEY, AND E. J. RIPLING. 1967. Use of crack-line-loaded specimens for measuring plane-strain fracture toughness. J. Mater. 2(3):661–681.

———, AND E. J. RIPLING. 1971. The fracture toughness and stress corrosion cracking characteristics of an anhydride-hardened epoxy adhesive. J. Appl. Poly. Sci. 15:641–659.

RIPLING, E. J., S. MOSTOVOY, AND R. L. PATRICK. 1963. Application of fracture mechanics to adhesive joints in Adhesion, ASTM, STP 360:5–16.

———, ———, AND ———. 1964. Measuring fracture toughness of adhesive joints. Mater. Res. Stand. 64(3):129–134.

———, H. T. CORTEN, AND S. MOSTOVOY. 1971. Fracture mechanics: a tool for evaluating structural adhesives. J. Adhes. 3:107–123.

STUMBO, D. A. 1960. Surface-texture measurements for quality and production control. For. Prod. J. 10(2):122–124.